

THE ORIGIN OF THE ULTRALUMINOUS X-RAY SOURCES

GRZEGORZ WIKTOROWICZ^{1,7}, MALGORZATA SOBOLEWSKA², JEAN-PIERRE LASOTA^{3,6,7}, KRZYSZTOF BELCZYNSKI^{1,5,7}

¹ Astronomical Observatory, Warsaw University, Al. Ujazdowskie 4, 00-478 Warsaw, Poland (gwiktoro@astrouw.edu.pl)

² Harvard-Smithsonian Center for Astrophysics, 60 Garden Street, Cambridge, MA 02138, USA

³ Nicolaus Copernicus Astronomical Center, Bartycka 18, 00-716 Warsaw, Poland

⁴ MIT Kavli Institute for Astrophysics and Space Research 77 Massachusetts Ave, Cambridge, MA 02139, USA

⁵ Warsaw Virgo Group

⁶ Institut d'Astrophysique de Paris, CNRS et Sorbonne Universités, UPMC Paris 06, UMR 7095, 98bis Bd Arago, 75014 Paris, France

⁷ Kavli Institute for Theoretical Physics, Kohn Hall, University of California, Santa Barbara, CA 93106, USA

Draft version May 18, 2017

ABSTRACT

Recently, several ultraluminous X-ray (ULX) sources were shown to host a neutron star (NS) accretor. We perform a suite of evolutionary calculations which show that, in fact, NSs are the dominant type of ULX accretor. Although black holes (BH) dominate early epochs after the star-formation burst, NSs outweigh them after a few 100 Myr and may appear as late as a few Gyr after the end of the star formation episode. If star formation is a prolonged and continuous event (i.e., not a relatively short burst), NS accretors dominate ULX population at any time in solar metallicity environment, whereas BH accretors dominate when the metallicity is sub-solar. Our results show a very clear (and testable) relation between the companion/donor evolutionary stage and the age of the system. A typical NS ULX consists of a $\sim 1.3 M_{\odot}$ NS and $\sim 1.0 M_{\odot}$ Red Giant. A typical BH ULX consist of a $\sim 8 M_{\odot}$ BH and $\sim 6 M_{\odot}$ main-sequence star. Additionally, we find that the very luminous ULXs ($L_X \gtrsim 10^{41}$ erg/s) are predominantly BH systems ($\sim 9 M_{\odot}$) with Hertzsprung gap donors ($\sim 2 M_{\odot}$). Nevertheless, some NS ULX systems may also reach extremely high X-ray luminosities ($\gtrsim 10^{41}$ erg/s).

Subject headings: stars: black holes, neutron stars, X-ray binaries

1. INTRODUCTION

Ultraluminous X-ray source (ULX; for review see Feng & Soria 2011) is defined by two observational properties:

1. it is a point-like (i.e. not extended) off-nuclear X-ray source with a peak emission localized in the X-ray band;
2. it emits isotropic equivalent X-ray luminosity in excess of 10^{39} erg s⁻¹, which is approximately the Eddington limit (EL) for a spherically accreting stellar-mass black hole (sMBH; $\sim 10 M_{\odot}$).

Until recently the main problem with unveiling the nature of the ULXs stemmed from the absence of reliable measurements of the masses of the accreting compact objects. This has changed with the discovery of pulsing ultraluminous X-ray sources (PULXs) which contain neutron stars (NS). The first X-ray pulsar was discovered in M82 X-2 (Bachetti et al. 2014). Then, two other PULXs have been identified: P13 in NGC 7793 (Fürst et al. 2016; Israel et al. 2017b), and NGC5907 ULX1, (Israel et al. 2017a; Fürst et al. 2017). All these PULXs show regular pulses with periods ~ 1 s, characteristic of NS accretors.

These discoveries proved that some ULXs do contain stellar-mass compact objects. Moreover, it is possible that NSs may reside in a vast majority of the ULXs (NSULXs; Kluźniak & Lasota 2015; King & Lasota 2016; King et al. 2017). Existence of PULXs provides strong evidence in support of the models involving a super-Eddington accretion onto a compact star (e.g., Begelman 2002; Poutanen et al. 2007; King 2009) as an explanation of the ULXs phenomenon (e.g. Kōrding et al. 2002).

However, apparent super-Eddington luminosities can also be reached without breaching the EL if the radiation of an accreting compact star is beamed (e.g., King et al. 2001; Poutanen et al. 2007). Detailed accretion disk simulations appear to support the importance of beaming (e.g., Ohsuga 2012; Jiang et al. 2014; Sądowski & Narayan 2015).

In this study we perform massive simulations in order to uncover the nature of the stars forming the ULX population. Motivated by the recent observational progress, we limited our investigation to the stellar-mass compact objects with super-Eddington and/or beamed emission.

2. SIMULATIONS

The calculations were performed with the use of **StarTrack** population synthesis code (Belczynski et al. 2002, 2008) with significant updates described in Dominik et al. (2012); Wiktorowicz et al. (2014).

We start the evolution of each system from the Zero Age Main Sequence (ZAMS), which we assume to happen at the same moment for both stars. The primary has an initial mass of $M_a = 6 - 150 M_{\odot}$ drawn from a power-law distribution with index -2.7 (Kroupa & Weidner 2003). The mass of the secondary (M_b) is chosen from the $0.08 - 150 M_{\odot}$ range to preserve a uniform mass-ratio distribution. Typical predecessors of X-ray binaries (XRB) with NS or BH accretors should reside in such a range of masses. The initial separations are uniform in logarithm ($P(a) \sim 1/a$; Abt 1983). The eccentricities' distribution is the thermal-equilibrium (Duquennoy & Mayor 1991). The binary fraction was set to 50% for stars with ZAMS mass below $10 M_{\odot}$ and 100% for systems with more massive primaries. We are aware of the results of Sana et al. (2012) who provide other relations

for initial parameters distributions, but their results were obtained for stars with masses $15 - 60 M_{\odot}$ and were limited to solar metallicity. Therefore, we decided to keep the previously established distributions. For comparison between our adopted and Sana et al. (2012) initial distributions the reader may refer to de Mink & Belczynski (2015).

We simulated the evolution of 2×10^7 binary systems for every model and scaled the results to the Milky-Way equivalent galaxy ($M_{\text{MWEG}} = 6 \times 10^{10} M_{\odot}$ (Licquia & Newman 2015); star formation rate (SFR) equal $6.0 M_{\odot} \text{ yr}^{-1}$ for constant star formation (SF) during 10 Gyr, and $600 M_{\odot} \text{ yr}^{-1}$ for burst SF with duration of 100 Myr). We do our study for solar metallicity (Z_{\odot}), 10% of solar ($Z_{\odot}/10$), and 1% of solar ($Z_{\odot}/100$).

2.1. Accretion model

We implemented a model based on nonlinear scaling of X-ray luminosity and mass accretion rate (e.g. Shakura & Sunyaev 1973),

$$L_{X,\text{tot}} = L_{\text{Edd}}(1 + \ln \dot{m}), \quad (1)$$

where \dot{m} is the mass transfer (MT) rate in Eddington rate units. Mass accretion onto compact object (\dot{M}_{acc}) is limited to \dot{M}_{Edd} and the rest of mass transferred to the system is lost in a wind from the inner disk region. Such outflows from ULXs were recently observed by Pinto et al. (2016).

2.2. Beaming model

The collimation of radiation from the innermost parts of the accretion disk, i.e. beaming, has a prodigious influence on the *apparent* isotropic luminosity. The beaming factor is defined as $b = \Omega/4\pi$, where Ω is the solid angle of emission (e.g. King et al. 2001). If we assume that there are two conical beams with opening angle θ , then $\Omega = 4\pi(1 - \cos \theta/2)$.

The isotropic equivalent X-ray luminosity (L_X) can be expressed as

$$L_X = \frac{L_{X,\text{tot}}}{b}. \quad (2)$$

Under assumption of the isotropic distribution of disk inclinations in space (see King 2009), the probability of observing a source along the beam is equal b .

The results of theoretical studies as well as the outcomes of detailed modeling of accretion disks favor the dependence of beaming on the mass transfer rate (e.g., Lasota 2016). King (2009) proposed that b scales as

$$\begin{aligned} b &\sim \frac{73}{\dot{m}^2} & \dot{m} &\geq 8.5, \\ b &= 1 & \dot{m} &< 8.5. \end{aligned} \quad (3)$$

For very high MT rates this prescription may give an extremely small value of b , i.e. strong beaming. For example, a Galactic ULX candidate SS433 has $\dot{m} \approx 3000 - 10^4$ (e.g. Fabrika 2004) for which Eqs. 3 and 2 give $b \approx 7 \times 10^{-7} - 8 \times 10^{-6}$ and $L_X \approx 10^{46} \text{ erg s}^{-1}$. Therefore, we will assume saturation at $\dot{m} = 150$. For higher mass accretion rates we will consider that the beaming

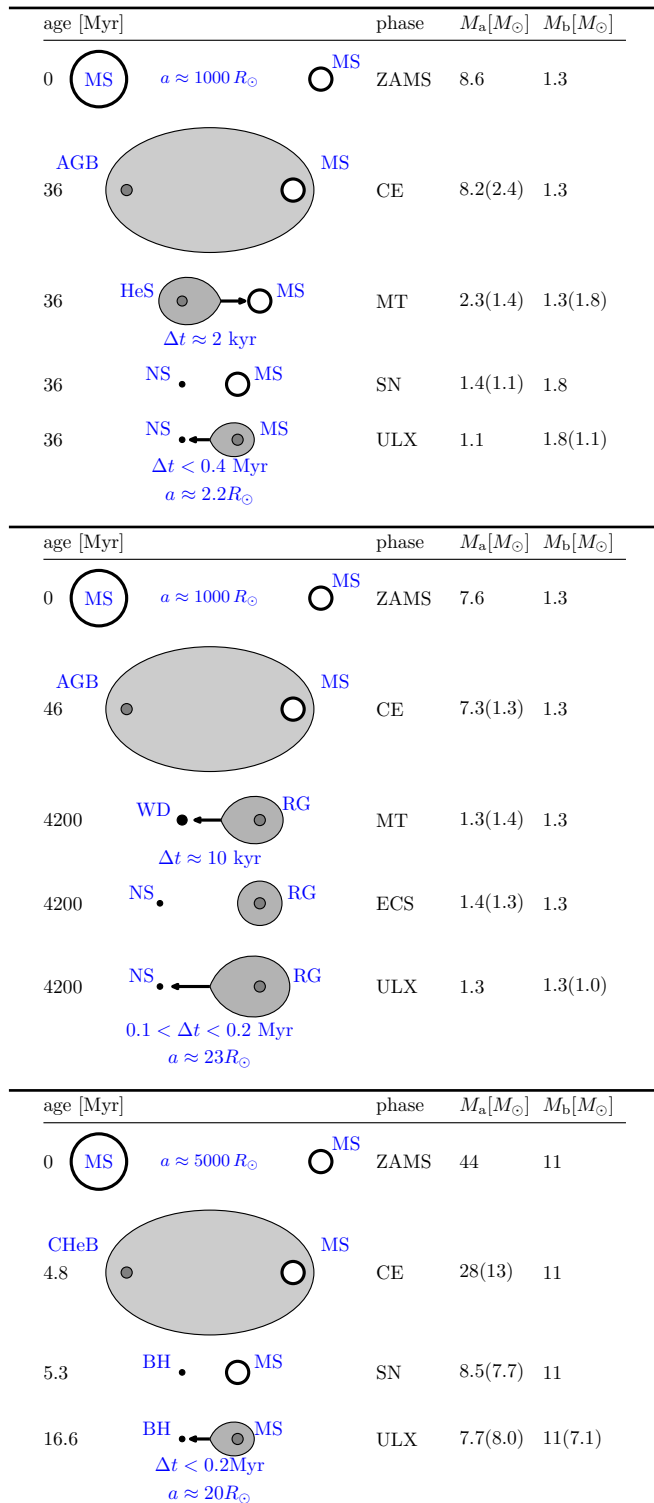


FIG. 1.— Schematic representation of the dominant NSULX evolutionary routes in young (top; $\mathcal{R}_{\text{NS,MS}}$) and old (middle; $\mathcal{R}_{\text{NS,RG}}$) stellar populations. Bottom: typical BHULX evolution (SF regions). The ages and masses reflect those in typical systems. For explanation of abbreviations see text (Sec. 3.1). Numbers in parentheses indicate change of component mass during a given stage.

is constant and equal $b \approx 3.2 \times 10^{-3}$ ($\theta \approx 9^\circ$). Theoretical background for beaming saturation was presented by Lasota et al. (2016).

3. RESULTS

TABLE 1
TYPICAL PARAMETERS OF ULXS

Route	t[Myr]	Δt [Myr]	Present			ZAMS		
			$M_a [M_\odot]$	$M_b [M_\odot]$	a[R_\odot]	$M_{ZAMS,a} [M_\odot]$	$M_{ZAMS,b} [M_\odot]$	$a_{ZAMS} [R_\odot]$
$Z = Z_\odot$								
$\mathcal{R}_{BH,MS}$	10–21	< 0.2	7.7–8.6	5.9–7.2	18–22	40–50	6.6–12	3800–4600
<i>ev. route:</i>	CE1(4-1;7/8-1)		SN1 MT2(14-1)					
$\mathcal{R}_{NS,MS}$	6–700	< 0.4	1.1–1.3	1.1–1.4	2.2–3.6	8.2–9.3	1.3–1.7	700–1200
<i>ev. route:</i>	CE1(3/4/5-1;7/8-1)		SN1 MT2(13-1)					
$\mathcal{R}_{NS,HG}$	700–1100	0.3–0.8	~ 1.3	0.6–1.0	7.3–17	7.9–8.3	1.6–2.0	800–1200
<i>ev. route:</i>	CE1(3/4/5-1;7/8-1)		SN1 MT2(13-1/2)					
$\mathcal{R}_{NS,RG}$	2400–4400	0.1–0.2	~ 1.3	~ 1.0	35–50	7.5–7.9	1.2–1.5	1100–1700
<i>ev. route:</i>	CE1(6-1;12-1)		MT2(12-3) AICNS1 MT2(13-3)					
$Z = Z_\odot/10$								
$\mathcal{R}_{BH,MS}$	4–40	< 27	5.7–8.9	5.6–7.8	14–19	26–37	6.0–11	1800–3700
$\mathcal{R}_{NS,MS}$	9–55	< 0.8	1.1–1.3	1.2–1.5	1.6–2.7	7.2–12	1.5–1.9	1000–2600
$\mathcal{R}_{NS,HG}$	570–1000	< 0.6	1.2–1.3	0.6–0.9	9.3–22	6–8	1.3–1.8	600–1500
$\mathcal{R}_{NS,RG}$	700–2100	< 0.1	~ 1.3	~ 1.0	35–45	6.3–6.8	1.3–1.6	1700–2700
$Z = Z_\odot/100$								
$\mathcal{R}_{BH,MS}$	7.2–18	< 1.0	12–21	7–11	12–17	35–55	9.1–14	540–2000
$\mathcal{R}_{NS,MS}$	470–800	0.6–1.3	1.2–1.4	0.9–1.0	2.8–3.5	7.2–8.2	1.7–2.0	500–900
$\mathcal{R}_{NS,HG}$	430–770	< 0.4	~ 1.3	0.6–0.8	17–35	6.0–6.3	1.7–2.1	700–900
$\mathcal{R}_{NS,RG}$	540–1600	< 0.1	~ 1.3	~ 1.0	30–45	6.0–6.2	1.3–1.7	900–1300

NOTE. — Typical present and ZAMS parameters of most common ULX evolutionary routes. Ranges represent 50% of values in present day populations. The parameter columns represent respectively: Age of the system in ULX phase (t), duration of ULX phase (Δt), compact object mass (M_a), donor mass (M_b), separation (a), primary mass on ZAMS ($M_{ZAMS,a}$), secondary mass on ZAMS ($M_{ZAMS,b}$), separation on ZAMS (a_{ZAMS}). The schematic evolutionary routes provided for $Z = Z_\odot$ are the same for other metallicities. Symbols meaning (Belczynski et al. 2008): CE1 - common envelope (donor: primary); MT2 - mass transfer (donor: secondary); SN1 - supernova (primary); AICNS1 - accretion induced collapse (primary); 1 - MS; 2 - HG; 3 - RG; 4 - CHeB; 5 - early AGB; 6 - thermal-pulsing AGB; 7 - HeS; 8 - evHeS; 12 - ONeWD; 13 - NS; 14 - BH.

3.1. Formation of NSULXs

According to our results, NSULX are present in ULX populations of all ages and metallicities. The first NSULXs form as early as ~ 6 Myr after the start of SF, but the ULX phase may occur also in a very old system ($t_{\text{age}} \sim 5$ Gyr). Dominant evolutionary routes leading to the occurrence of high MT rate and formation of a NSULX depend on the age of the system at the time of the ULX phase. Below we describe the typical routes for early ($\mathcal{R}_{NS,MS}$), mid-age ($\mathcal{R}_{NS,HG}$), and old ($\mathcal{R}_{NS,RG}$) stellar populations (see also Fig. 1). Ranges represent 50% of values in present day populations¹.

6–800 Myr; Route $\mathcal{R}_{NS,MS}$; Typical companion MS— On ZAMS the masses of the primary and secondary are $7.2–12 M_\odot$ and $1.3–2.0 M_\odot$, respectively. The initial separation, $500–2600 R_\odot$, shrinks during the CE phase commenced by the primary. After the CE phase, the primary forms a NS through a core collapse supernova explosion (SN). The natal kick leaves the system on an orbit that is tight enough for the secondary to fill its Roche lobe due to nuclear expansion and gravitational radiation (GR) before it leaves the main sequence (MS). During the RLOF the companion is comparable in mass ($0.9–1.5 M_\odot$) to the NS ($1.1–1.4 M_\odot$), thus the MT is stable and may be sustained as long as ~ 1.3 Myr (see Fig. 1, top).

430–1100 Myr; Route $\mathcal{R}_{NS,HG}$; Typical companion HG— In approximately 54–73% percent of the systems following the $\mathcal{R}_{NS,MS}$ route the RLOF during the MS phase,

¹ i.e., population as we predict them to look like for an observer able to see all the objects at the same time. Problems related to light propagation (e.g. light speed, interstellar absorption) are not discussed in this study.

if present, is not strong enough to power an ULX. These secondaries start to reach their terminal-age MS and expand rapidly several hundred Myr after the start of the SF. If the separation is short enough, they will fill their RL. Thus, at this time, a Hertzsprung-Gap (HG) star becomes the most common NSULX companion.

540–4400 Myr; Route $\mathcal{R}_{NS,RG}$; Typical companion RG— The evolution of the late-time NSULXs is significantly different than that of the earlier ULXs. After a CE phase the primary forms an Oxygen-Neon White Dwarf (ONeWD) instead of a NS, and thus the mass of the primary is on average lower compared with routes $\mathcal{R}_{NS,MS}$ and $\mathcal{R}_{NS,HG}$. However, when the secondary becomes a Red Giant (RG) and fills its RL of $\sim 10–20 R_\odot$, the primary accretes additional mass and forms a NS due to an accretion induced collapse (AIC). Afterwards, the RG refills its RL and a short ULX phase occurs (Fig. 1, middle).

3.1.1. Formation of BHULXs

In general, BHULXs are a minority in our results. Nevertheless, they dominate the ULX population during the initial phase of the constant SF (exception being population with low ($\leq Z_\odot/10$) metallicity), and during the SF burst. They are also more numerous than NSULXs among the ULXs with luminosity in excess of 10^{41} erg s⁻¹ (see Secs. 3.2 and 3.3).

4–40 Myr; Route $\mathcal{R}_{BH,MS}$; Typical companion MS— The initial binary on ZAMS consist of a massive primary ($26–55 M_\odot$) and an intermediate-mass secondary ($6–14 M_\odot$). The initial semi-major axis is $\sim 540–4000 R_\odot$.

The heavier star evolves very quickly and during the CHeB phase fills its RL commencing the CE episode.

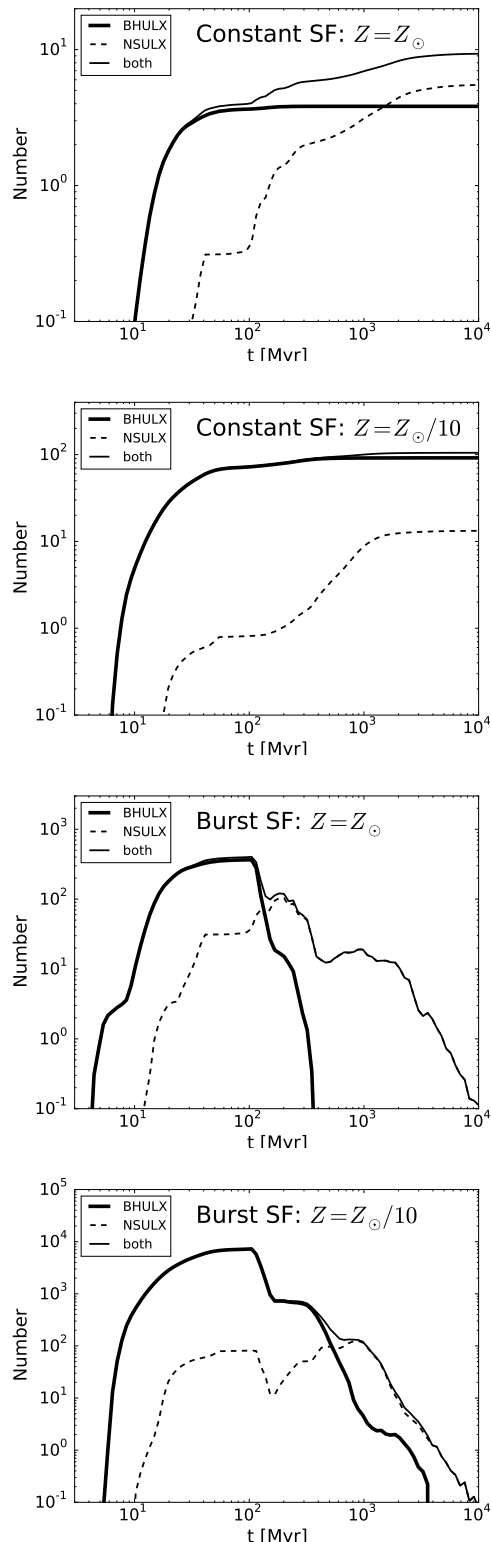


FIG. 2.— Time evolution of the number of ULXs since the beginning of star formation. The BHULXs (thick line) appear early, but 100–1000 Myr later the ULX population becomes dominated by the NSULXs (dashed line), except constant SF models with sub-solar metallicities. Number of ULXs for a star forming mass of $6 \times 10^{10} M_{\odot}$ (see Sec. 2).

As a result, the primary is deprived of its hydrogen envelope and the separations drops to a few $\times 10 R_{\odot}$. A

direct collapse occurs shortly afterwards. The combined action of the companion’s nuclear expansion and gravitational radiation (GR) leads to a RLOF. The phase of ULX emission is short, $\lesssim 1.0$ Myr (Fig. 1, bottom).

3.2. Number of ULXs

By the number of ULXs ($\#ULX$) we understand the predicted number of observed systems at the present time. We find that $\#ULX$ strongly depends on the SFR history (Fig. 2).

Constant SFR naturally leads to a constant growth in $\#ULX$, which starts early after the start of SF (~ 5 Myr) and after a few Gyr reaches a constant value of $\#ULX = 9.3, 100,$ and 56 for $Z_{\odot}, Z_{\odot}/10,$ and $Z_{\odot}/100$, respectively (see Sec. 4.2).

BHULXs appear first in both constant and burst SF scenarios. In the former case, the number of BHULXs increases to the age of a few hundreds Myr, at which time it reaches a constant value of 3.8, 92, 51 for $Z_{\odot}, Z_{\odot}/10,$ and $Z_{\odot}/100$, respectively. In the case of a burst SF, the formation time of BHULXs is limited nearly exactly to the duration of the burst ($\lesssim 200$ Myr).

NSULXs resulting from different evolutionary routes described in Sec. 3.1 appear sequentially in their chronological order and form the characteristic steep sections (constant SF) or humps (burst SF) at ~ 100 Myr ($\mathcal{R}_{NS,MS}$), ~ 200 Myr ($\mathcal{R}_{NS,HG}$), and ~ 1 Gyr ($\mathcal{R}_{NS,RG}$).

ULX populations younger than ~ 100 Myr are dominated by the BHULX. For constant SF, the NSULXs become more abundant than the BHULXs (58% of the ULX accretors) only if $Z = Z_{\odot}$. For lower metallicities, the $\#BHULX$ grows rapidly during the first few hundreds Myr whereas the rate of the NSULXs formation is much lower, and they are not able to match the abundance of the BHULXs during the next 10 Gyr. As a result, the NSULXs account for not more than $\sim 12\%$ and $\sim 8\%$ of all ULXs for $Z_{\odot}/10$ and $Z_{\odot}/100$, respectively. However, for burst SF and all investigated metallicities, the NSULXs exceed the BHULXs in numbers within $\lesssim 1$ Gyr, and after a few Gyr they become the only surviving ULXs.

3.3. ULXs with luminosities exceeding $10^{41} \text{ erg s}^{-1}$

Several surveys found a break in the X-ray luminosity function (XLF) at $\lesssim 10^{41} \text{ erg s}^{-1}$, which may point toward a different populations below and above this luminosity (e.g., Grimm et al. 2003; Swartz et al. 2011; Mineo et al. 2012). Thus, it is interesting to point out that hyper-luminous X-ray sources (HLX) defined as ULXs with $L_X \gtrsim 10^{41} \text{ erg s}^{-1}$ have different donors than the ULXs with $L_X \ll 10^{41} \text{ erg s}^{-1}$. We find that 52–84% of the ULXs (described in Sec. 3) have luminosities in the range $(1-3) \times 10^{39} \text{ erg s}^{-1}$.

Approximately 90% of HLXs are BHULXs with HG donors. NS accretors in HLXs may obtain nearly as high luminosities as BH accretors and are typically accompanied by evolved helium stars (evHeS). Noteworthy, the evolutionary HLX routes match those reported for HLXs with $L_X \geq 10^{42} \text{ erg s}^{-1}$ in Wiktorowicz et al. (2015). The current results, however, are based on a much wider range of models and more physical treatment of NS/BH accretion, and we include here the HLX evolutionary paths for completeness. Notice that the PULX

NGC5907 ULX1 has a luminosity $\gtrsim 10^{41}$ erg s $^{-1}$ (Fuerst et al. 2016).

11–130 Myr; Route $\mathcal{R}_{\text{BH,HG}}$; Typical companion HG— A typical system begins its evolution as 25–50 M_{\odot} primary with a 5–10 M_{\odot} companion. After ~ 5 Myr and the loss of 1–10 M_{\odot} in stellar wind the primary fills the RL as a CHeB star and commences the CE phase. It loses a large fraction of its mass ($\sim 50\%$), but the separation shrinks to $\sim 15 R_{\odot}$. After additional ~ 0.5 Myr a ~ 7 –18 M_{\odot} BH forms in a direct collapse. The secondary becomes a HG star ~ 10 –55 Myr later and it expands rapidly. Shortly after, it fills its RL and starts the MT. For a short time (< 0.08 Myr) the MT is high enough to power a ULX with $L_X > 10^{40}$ erg s $^{-1}$ (see Fig. 3, top).

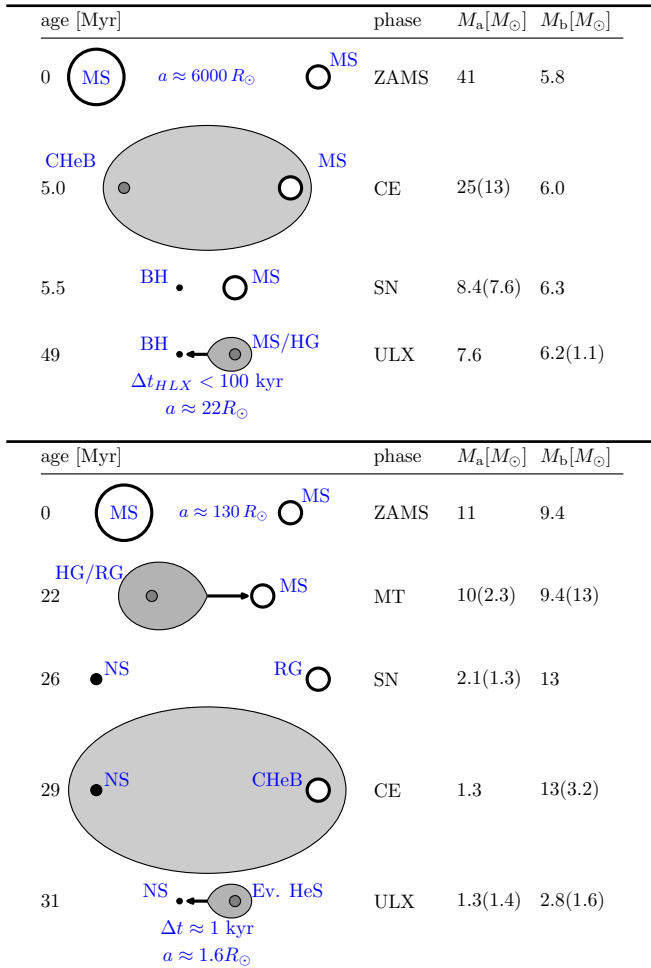


FIG. 3.— Schematic description of the evolution of the most luminous ($L_X > 10^{41}$ erg s $^{-1}$) ULXs. Top/bottom plot is for a BH/NS accretor. The numbers depict parameters of a typical system.

27–300 Myr; Route $\mathcal{R}_{\text{NS,evHeS}}$; Typical companion evHeS— The stars on ZAMS are less massive and have smaller mass ratio than in the case of $\mathcal{R}_{\text{BH,HG}}$. When the primary fills the RL as a RG, the MT is stable and proceeds for a few tens of kyr. The donor loses most of its hydrogen envelope and after a few Myrs at the age of ~ 25 Myr it forms a NS through a SN explosion. The companion, being a RG, expands and fills its RL. This time the MT is unstable due to a high mass ratio and the CE occurs. Af-

terwards, the secondary becomes a low-mass (a few Solar masses) helium star (HeS). The secondary continues its evolution for the next few Myrs, expands and fills its RL again. This time, although being very strong, the MT is stable and for ~ 1 kyr it powers an HLX (see Fig. 3, bottom).

The *appendix* contains the most important characteristics of the simulated population of ULXs for different models: the evolution of #ULX after the burst SF (Tab. 4), the dependence of #ULX on $L_{X,\text{min}}$ (Tab. 5) the distributions of general population’s parameters (Tabs. 6, 7, 8, 9, and 10); the evolution of the #ULX through population age (Figs. 5 and 6); and the distributions of companions (Tabs. 11, 12, 13, 14, and 15).

4. DISCUSSION

ULXs are observed in all kinds of galaxies (e.g. Mushotzky 2006). However, ULXs appear to be more abundant in the star-forming galaxies than in the elliptical galaxies (e.g. Irwin et al. 2004; Swartz et al. 2004; Feng & Soria 2011; Wang et al. 2016, however see Soria 2007). In addition, ULXs are commonly detected in star-burst regions (e.g., Fabbiano et al. 2001; Gao et al. 2003). Feng & Soria (2011) pointed out that this connection is particularly valid for the most luminous ULXs. On the contrary, Mushotzky (2006) performed a direct examination of the ULXs’ positions and found that approximately 1/3 of them had to form outside of the star-forming regions.

These observations may be understood on the ground of our results. On the one hand, spatial correlation of ULXs and SF regions is expected because during the SF episodes ULXs form mainly through routes $\mathcal{R}_{\text{BH,MS}}$ and $\mathcal{R}_{\text{NS,MS}}$, which produce numerous sources early after the start of SF. Additionally, the most luminous ULXs (HLXs) formed in our simulations evolve from heavier stars at an early age ($t_{\text{age}} \lesssim 200$ Myr). On the other hand, the ULX phase in systems formed outside the SF regions occurs later on after ZAMS ($\mathcal{R}_{\text{NS,HG}}$, $\mathcal{R}_{\text{NS,RG}}$). However, we found that these late-time ULXs constitute only 1–10% of all ULXs for constant SF.

4.1. NS accretors in ULXs

Our results predict a large fraction of NS accretors among the ULXs. Current observational status is consistent with our results. The discovery of the first NSULX (Bachetti et al. 2014) proved that apparent luminosities orders of magnitude larger than the Eddington limit are possible in nature. Kluźniak & Lasota (2015) proposed that the M82 X-1 and the P13 in NGC 7793 may be also PULXs. Following discoveries (Fuerst et al. 2016; Israel et al. 2017a) showed that NSs may indeed be widespread among the ULXs. Finally, a known X-ray pulsar SMC X-3 was reported to reach an outburst luminosity of 2.5×10^{39} erg s $^{-1}$ (Tsygankov et al. 2017). Pin-tore et al. (2017) argued that the energy spectra of several ULXs can be explained with a ‘pulsator-like’ continuum model used to describe Galactic XRBs containing NSs (e.g. White et al. 1995; Coburn et al. 2001).

Theoretical considerations further support our findings. King & Lasota (2016) showed that a ULX with a weakly magnetized NS and a ULX with a BH may be observationally hard to distinguish if the NS does not

TABLE 2
TYPICAL PARAMETERS OF HLXS

Route	t[Myr]	Δt [Myr]	Present $M_a [M_\odot]$	$M_b [M_\odot]$	$a [R_\odot]$	$M_{ZAMS,a} [M_\odot]$	ZAMS $M_{ZAMS,b} [M_\odot]$	$a_{ZAMS} [R_\odot]$
$\mathcal{R}_{BH,HG}$	15–40	$\lesssim 0.08$	8.0–10	1.7–3.3	$Z = Z_\odot$ 20–90	40–50	3.8–8.2	3700–4600
$\mathcal{R}_{NS,evHeS}$	17–40	$\lesssim 0.001$	1.3–1.4	1.7–2.6	$\lesssim 4.4$	10–11	8.5–10	30–300
	MT1(2/3/4/5/6-1/2/4) SN1		CE2(13-3/4/5;13-7/8) MT2(14-1/2)		$Z = Z_\odot/10$			
$\mathcal{R}_{BH,HG}$	20–60	$\lesssim 0.06$	7.2–9.5	1.7–3.3	12–120	25–35	4.0–7.0	2000–5000
$\mathcal{R}_{NS,evHeS}$	40–60	$\gtrsim 0.001$	~ 1.3	1.5–2.0	8.4–13	8.8–9.5	5.5–7.3	170–430
					$Z = Z_\odot/100$			
$\mathcal{R}_{BH,HG}$	20–45	$\lesssim 0.04$	10–18	1.2–3.7	10–75	25–45	5.0–9.0	700–2600
$\mathcal{R}_{NS,evHeS}$	50–75	$\gtrsim 0.001$	~ 1.3	1.9–2.5	2.1–6.9	6.4–6.8	5.5–6.2	170–280

NOTE. — Typical present and ZAMS parameters of typical most luminous ULXs (HLX; routes $\mathcal{R}_{BH,HG}$ and $\mathcal{R}_{NS,evHeS}$). The table is organized in the same way as Tab. 1.

pulsate. King et al. (2017) argued that the conditions for pulsations in PULXs are relatively strict and a large population of NSULXs will mimic the BHULXs.

The significant number of NSULX that follows from most of our simulated models may be understood on the statistical ground. While it is easier to obtain large MT rates in the BHULXs, the NSULXs progenitors are more abundant in the ZAMS distributions. In general, NSs form from stars with ZAMS masses ~ 8 – $22 M_\odot$, whereas BH form from more massive stars with ~ 22 – $150 M_\odot$. For $\alpha_{IMF} = -2.7$ it gives the ratio of NS to BH progenitors of ~ 4.8 , and for $\alpha_{IMF} = -2.3$ this ratio is 3.0. Moreover, in the NSULX route which dominates in the old stellar populations ($\mathcal{R}_{NS,RG}$) the primary on ZAMS may have even lower mass of $\sim 6 M_\odot$, which gives the ratio of NS to BH progenitors of 4.8 for $\alpha_{IMF} = -2.3$. It first becomes a WD before accreting mass and collapsing into a NS. Additionally, donors in NSULXs are less massive than in BHULXs and, therefore, also more abundant on ZAMS. We note that low mass donors may occur also in BHULXs, but it is far harder (and therefore less probable) for them to survive the CE. Even if they succeeded, the post-CE separation is so small that the RLOF occurs earlier than typically for NSULXs. All these results in a significantly smaller number of BHULXs with low-mass ($\lesssim 2 M_\odot$) donors than in NSULXs.

During short SF episodes, the ULX population is dominated by sources with BH accretors. BHs may acquire stable MT from heavier companions than NSs. Heavier stars expand more and faster, therefore, BHULXs age during ULX phase is of the order of ~ 10 Myr, whereas for NSULX it is ~ 100 Myr (route $\mathcal{R}_{NS,MS}$). As a result BHULXs appear in larger numbers in the first ~ 100 Myr. The ULX phase may appear in NSULX as early as ~ 10 Myr after ZAMS. However, it demands a very specific pre-CE conditions, which occur in a relatively narrow ZAMS parameter space. For an average post-CE separation in early NSULXs ($\mathcal{R}_{NS,MS}$) the star needs ~ 100 Myr to fill its RL.

The picture is different for the constant SF or long bursts. As the SF continues, the $\#BHULX$ saturates for ~ 200 Myr after the SF start, because at this time comparable number of sources begin and end their ULX phase. However, a significant number of NSULXs have their ULX phases during the post-MS expansion of their

light donors. Therefore, the $\#NSULX$ grows continuously for several Gyr and new NSULX formation routes appear successively (see Sec. 3.1 for the sequence). For $Z = Z_\odot$, the $\#NSULX$ becomes higher than $\#BHULX$ after ~ 1 Gyr. However, for lower metallicities, $\#NSULX$ does not overcome $\#BHULX$ within 10 Gyr.

When the SF is extinguished, $\mathcal{R}_{BH,MS}$ quickly disappear as their massive donors end their lives fast ($\lesssim 500$ Myr). On the other hand, NSULXs with low-mass donors may commence the ULX phase after several Gyr of evolution when the secondary fills the RL during the post-MS expansion ($\mathcal{R}_{NS,HG}$ and $\mathcal{R}_{NS,RG}$). Therefore, after the end of the SF, NSULXs quickly (in ~ 100 Myr) become the dominant ULXs and after ~ 1 Gyr BHULXs disappear completely.

The population synthesis of NSULXs was recently performed with the use of BSE code by Fragos et al. (2015). However, they omitted the pre-SN evolution and explored a far smaller parameter space than that presented in this work. Even though they utilized the MESA code to calculate the MT rates, their maximum values are similar to ours ($\dot{M} \lesssim 10^{-2}$ Myr). We obtained less massive companions in NSULXs, but (Fragos et al. 2015) focused on M82 X-2 source with companion mass $\gtrsim 5.2 M_\odot$ (Bacchetti et al. 2014) and assumed that heavier stars are necessary to survive the CE phase.

Shao & Li (2015) also took the population synthesis approach to study NSULXs and found a significant population of these sources. They adopted a realistic envelope’s binding energy from Xu & Li (2010), but considered only a solar metallicity and constant beaming of $b = 0.1$.

4.2. Dependence of $\#ULX$ on Metallicity

Observations show that ULXs are often associated with low metallicity environments (e.g. Pakull & Mirioni 2002; Soria et al. 2005; Luangtip et al. 2015; Mapelli et al. 2010). Many authors have demonstrated that in a low metallicity environment it is easier to form a massive BH (e.g., Zampieri & Roberts 2009; Mapelli et al. 2009; Belczynski et al. 2010), and it is more common to obtain a RLOF onto a compact object (Linden et al. 2010).

In this study we find that the metallicity has a strong impact on $\#ULX$, but only in SF regions (See Tab. 4). We show that the number of $\#BHULX$ increases significantly for $Z_\odot/10$ in comparison to Z_\odot . However, the

#NSULX is virtually unaffected by metallicity. Interestingly, for models with the lowest investigated metallicity ($Z_{\odot}/100$) we found fewer ULXs than for $Z = Z_{\odot}/10$. Therefore, our results suggest that the relation $\#ULX(Z)$ is not monotonic (see Prestwich et al. 2013). We plan to study this outcome in more details in a forthcoming publication (Wiktorowicz et al. in preparation).

4.3. Counterparts

Several searches were performed to directly observe the ULX companions. However, only a handful have been detected among hundreds of known ULXs. Additionally, ULXs, being extra-galactic objects, are observationally biased towards more luminous and therefore more massive companions. In our results, NS counterparts in ULX are predominantly low-mass ($\lesssim 1.5 M_{\odot}$) stars. If located in other galaxies, such objects would be hard to detect. This may explain why it is hard to find counterparts to majority of the ULXs.

Some ULXs were observed near OB stars (e.g. Soria et al. 2005). Such stars are too massive to provide a stable MT to a NS accretor, so they may only be accompanied by BH accretors, unless the MT occurs through a stellar wind (Not considered in our study). OB stars evolve quickly (< 100 Myr), which suggests that they should be spatially associated with the SF regions, where the BHULXs are more numerous than the NSULXs according to our results. Typical BHULX companions in our simulations are MS stars of $5.6 - 11 M_{\odot}$, which matches the B spectral type.

Roberts et al. (2008) found 5 potential optical ULX companions with the use of the Hubble Space Telescope. The optical search for companions in ULXs was performed also by Gladstone et al. (2013) who used the same instrument and found 13 ± 5 counterparts to ULXs located within a distance of $D \leq 5$ Mpc. Most of them were MS stars or RGs. A near-infrared (NIR) search was performed by Heida et al. (2014, 2016) who observed 62 ULXs in 37 galaxies located within 10 Mpc. They found 17 candidate counterparts, 13 of which are red supergiants.

The companion to NS ULX P13 in NGC7793 was detected and estimated to be a BI9a star with mass $18 - 23 M_{\odot}$ (Motch et al. 2014). Radius of such a star is $4 - 700 R_{\odot}$, depending on its evolutionary stage. Orbital period estimate ($P_{\text{orb}} = 64$ d) puts a Roche lobe radius of a donor at $\sim 120 R_{\odot}$ (under the assumption of circular orbit and $M_{\text{NS}} = 1.4 M_{\odot}$). The BI9a star may obtain such a radius during CHeB phase. According to a standard prescription, in a high mass-ratio system the RLOF will be unstable and the CE will occur. However, Pavlovskii et al. (2017) found that the range of stable mass ratios may be wider than previously thought. We will analyse this possibility in a separate study (Wiktorowicz et al. in preparation). BHULXs with high-mass donors may be predecessors of double BHs mergers (Belczynski et al. 2016).

5. SUMMARY AND CONCLUSIONS

We analyzed accretion onto compact stars in order to investigate the parameters and characteristics of the ULX population. We demonstrate that on the grounds of the current understanding of the accretion physics and stellar evolution we *are* able to reproduce the vast ma-

ajority of the observed population of ULXs without the need for intermediate-mass black hole accretors.

We performed a population synthesis study with the use of **StarTrack** population synthesis code to simulate 2×10^7 isolated binaries with initial parameters leading to the formation of XRBs (both LMXB and HMXB). Our simulation grid involves various accretion models, beaming prescriptions, and metallicities.

Our main conclusions are as follows:

- *ULX with NS accretors dominate the post-burst ULX populations*, and constant SF (duration > 1 Gyr) in high- Z environments, what is a natural consequence of the current understanding of the binary evolution. NSULXs are present in significant numbers ($\gtrsim 10\%$) also during the SF bursts and in lower- Z ULX populations.
- *ULXs appear in a very specific sequence after the start of the SF* (t depicts here the time since the beginning of the SF):
 1. $t \approx 4 - 40$ Myr BH-MS ($5.6 - 11 M_{\odot}$),
 2. $t \approx 6 - 800$ Myr NS-MS ($0.9 - 1.5 M_{\odot}$),
 3. $t \approx 430 - 1100$ Myr NS-HG ($0.6 - 1.0 M_{\odot}$),
 4. $t \approx 540 - 4400$ Myr NS-RG ($\sim 1.0 M_{\odot}$);
- *We found that NSULXs may reach luminosities as high as those of BHULXs* ($L_{\text{X,max}} > 10^{41} \text{ erg s}^{-1}$).
- *The most luminous ULXs* ($L_{\text{X}} \gtrsim 10^{41} \text{ erg s}^{-1}$) *contain HG donors* (BHULXs; $M_{\text{b}} \approx 1.2 - 3.7 M_{\odot}$) *or evolved helium stars*. (NSULXs; $M_{\text{b}} \approx 1.7 - 2.6 M_{\odot}$), which overflow their RL and transfer mass on thermal-timescale. They form typically within $15 - 75$ Myr since ZAMS.
- *The number of ULXs is anti-correlated with metallicity*. However, for very low- Z this relation changes sign.

We would like to thank volunteers whose participation in the Universe@Home project² made it possible to acquire the results in such a short time. This study was partially supported by the Polish NCN grants N203 404939, UMO-2015/19/B/ST9/01099 and by Polish NCN grant SONATA BIS 2. MS was supported by NASA contract NAS8-03060 (Chandra X-ray Center). MS acknowledges also the Polish National Science Centre grant UMO-2014/13/B/ST9/00570. JPL was supported in part by a grant from the French National Space Center CNES. KB acknowledges support from the Polish National Science Center (NCN) grants: Sonata Bis 2 (DEC-2012/07/E/ST9/01360), OPUS (2015/19/B/ST9/01099), OPUS (2015/19/B/ST9/03188) and MAESTRO (2015/18/A/ST9/00746) GW was supported by the grant No. UMO-2015/19/B/ST9/03188 and UMO-2014/14/M/ST9/0707. This research was supported in part by the National Science Foundation under Grant No. NSF PHY-1125915.

REFERENCES

- Abt, H. A. 1983, *ARA&A*, 21, 343
- Bachetti, M., Harrison, F. A., Walton, D. J., et al. 2014, *Nature*, 514, 202
- Begelman, M. C. 2002, *ApJ*, 568, L97
- Belczynski, K., Bulik, T., Fryer, C. L., et al. 2010, *ApJ*, 714, 1217
- Belczynski, K., Holz, D. E., Bulik, T., & O’Shaughnessy, R. 2016, *Nature*, 534, 512
- Belczynski, K., Kalogera, V., & Bulik, T. 2002, *ApJ*, 572, 407
- Belczynski, K., Kalogera, V., Rasio, F. A., et al. 2008, *ApJS*, 174, 223
- Coburn, W., Heindl, W. A., Gruber, D. E., et al. 2001, *ApJ*, 552, 738
- de Mink, S. E., & Belczynski, K. 2015, *ApJ*, 814, 58
- Dominik, M., Belczynski, K., Fryer, C., et al. 2012, *ApJ*, 759, 52
- Duquenois, A., & Mayor, M. 1991, *A&A*, 248, 485
- Fabbiano, G., Zezas, A., & Murray, S. S. 2001, *ApJ*, 554, 1035
- Fabrika, S. 2004, *Astrophysics and Space Physics Reviews*, 12, 1
- Feng, H., & Soria, R. 2011, *NAR*, 55, 166
- Fragos, T., Linden, T., Kalogera, V., & Sklias, P. 2015, *ApJ*, 802, L5
- Fuerst, F., Walton, D. J., Harrison, F. A., et al. 2016, *ArXiv e-prints*, arXiv:1609.07129
- Fürst, F., Walton, D. J., Stern, D., et al. 2017, *ApJ*, 834, 77
- Fürst, F., Walton, D. J., Harrison, F. A., et al. 2016, *ApJ*, 831, L14
- Gao, Y., Wang, Q. D., Appleton, P. N., & Lucas, R. A. 2003, *ApJ*, 596, L171
- Gladstone, J. C., Copperwheat, C., Heinke, C. O., et al. 2013, *ApJS*, 206, 14
- Grimm, H.-J., Gilfanov, M., & Sunyaev, R. 2003, *MNRAS*, 339, 793
- Heida, M., Jonker, P. G., Torres, M. A. P., et al. 2016, *MNRAS*, 459, 771
- . 2014, *MNRAS*, 442, 1054
- Irwin, J. A., Bregman, J. N., & Athey, A. E. 2004, *ApJ*, 601, L143
- Israel, G. L., Belfiore, A., Stella, L., et al. 2017a, *Science*, 355, 817
- Israel, G. L., Papitto, A., Esposito, P., et al. 2017b, *MNRAS*, 466, L48
- Jiang, Y.-F., Stone, J. M., & Davis, S. W. 2014, *ApJ*, 796, 106
- King, A., & Lasota, J.-P. 2016, *MNRAS*, 458, L10
- King, A., Lasota, J.-P., & Kluźniak, W. 2017, *MNRAS*, 468, L59
- King, A. R. 2009, *MNRAS*, 393, L41
- King, A. R., Davies, M. B., Ward, M. J., Fabbiano, G., & Elvis, M. 2001, *ApJ*, 552, L109
- Kluźniak, W., & Lasota, J.-P. 2015, *MNRAS*, 448, L43
- Körding, E., Falcke, H., & Markoff, S. 2002, *A&A*, 382, L13
- Kroupa, P., & Weidner, C. 2003, *ApJ*, 598, 1076
- Lasota, J.-P. 2016, in *Astrophysics and Space Science Library*, Vol. 440, *Astrophysics of Black Holes: From Fundamental Aspects to Latest Developments*, ed. C. Bambi, 1
- Lasota, J.-P., Vieira, R. S. S., Sądowski, A., Narayan, R., & Abramowicz, M. A. 2016, *A&A*, 587, A13
- Licquia, T. C., & Newman, J. A. 2015, *ApJ*, 806, 96
- Linden, T., Kalogera, V., Sepinsky, J. F., et al. 2010, *ApJ*, 725, 1984
- Luangtip, W., Roberts, T. P., Mineo, S., et al. 2015, *MNRAS*, 446, 470
- Mapelli, M., Colpi, M., & Zampieri, L. 2009, *MNRAS*, 395, L71
- Mapelli, M., Ripamonti, E., Zampieri, L., Colpi, M., & Bressan, A. 2010, *MNRAS*, 408, 234
- Mineo, S., Gilfanov, M., & Sunyaev, R. 2012, *MNRAS*, 419, 2095
- Motch, C., Pakull, M. W., Soria, R., Grisé, F., & Pietrzyński, G. 2014, *Nature*, 514, 198
- Mushotzky, R. 2006, *Advances in Space Research*, 38, 2793
- Ohsuga, K. 2012, in *Astronomical Society of the Pacific Conference Series*, Vol. 460, *AGN Winds in Charleston*, ed. G. Chartas, F. Hamann, & K. M. Leighly, 176
- Pakull, M. W., & Mirioni, L. 2002, *ArXiv Astrophysics e-prints*, astro-ph/0202488
- Pavlovskii, K., Ivanova, N., Belczynski, K., & Van, K. X. 2017, *MNRAS*, 465, 2092
- Pinto, C., Middleton, M. J., & Fabian, A. C. 2016, *Nature*, 533, 64
- Pintore, F., Zampieri, L., Stella, L., et al. 2017, *ApJ*, 836, 113
- Poutanen, J., Lipunova, G., Fabrika, S., Butkevich, A. G., & Abolmasov, P. 2007, *MNRAS*, 377, 1187
- Prestwich, A. H., Tsantaki, M., Zezas, A., et al. 2013, *ApJ*, 769, 92
- Roberts, T. P., Levan, A. J., & Goad, M. R. 2008, *MNRAS*, 387, 73
- Sana, H., de Mink, S. E., de Koter, A., et al. 2012, *Science*, 337, 444
- Sądowski, A., & Narayan, R. 2015, *MNRAS*, 453, 3213
- Sądowski, A., Narayan, R., McKinney, J. C., & Tchekhovskoy, A. 2014, *MNRAS*, 439, 503
- Shakura, N. I., & Sunyaev, R. A. 1973, *A&A*, 24, 337
- Shao, Y., & Li, X.-D. 2015, *ApJ*, 802, 131
- Soria, R. 2007, in *IAU Symposium*, Vol. 238, *Black Holes from Stars to Galaxies – Across the Range of Masses*, ed. V. Karas & G. Matt, 235–240
- Soria, R., Cropper, M., Pakull, M., Mushotzky, R., & Wu, K. 2005, *MNRAS*, 356, 12
- Swartz, D. A., Ghosh, K. K., Tennant, A. F., & Wu, K. 2004, *ApJS*, 154, 519
- Swartz, D. A., Soria, R., Tennant, A. F., & Yukita, M. 2011, *ApJ*, 741, 49
- Tsygankov, S. S., Doroshenko, V., Lutovinov, A. A., Mushtukov, A. A., & Poutanen, J. 2017, *ArXiv e-prints*, arXiv:1702.00966
- Wang, S., Qiu, Y., Liu, J., & Bregman, J. N. 2016, *ApJ*, 829, 20
- White, N. E., Nagase, F., & Parmar, A. N. 1995, *X-ray Binaries, 1* Wiktorowicz, G., Belczynski, K., & Maccarone, T. 2014, in *Binary Systems, their Evolution and Environments*, 37
- Wiktorowicz, G., Sobolewska, M., Sądowski, A., & Belczynski, K. 2015, *ApJ*, 810, 20
- Xu, X.-J., & Li, X.-D. 2010, *ApJ*, 722, 1985
- Zampieri, L., & Roberts, T. P. 2009, *MNRAS*, 400, 677

APPENDIX

DETAILS OF THE SIMULATIONS

If not stated differently, throughout the article a ‘luminosity’ means an X-ray luminosity in the 0.2–10 keV band. We do not take into account NS magnetic fields and include only non-rotating BHs.

We utilized the EL for luminosity (L_{Edd}) and mass accretion (\dot{M}_{Edd}) as

$$L_{\text{Edd}} = \eta \dot{M}_{\text{Edd}} c^2 = 2.51 \times 10^{38} \text{ erg s}^{-1} \frac{1}{1+X} \left(\frac{\dot{M}_{\text{acc}}}{M_{\odot}} \right), \quad (\text{A1})$$

where $\eta = 1/12$ for BH accretors and ~ 0.2 for NSs, X is a fraction of Hydrogen in the envelope of the donor. $X = 0.7$ for hydrogen rich donors and $X = 0$ for HeS and WD.

Most of the results are provided as present time distributions. This means the distributions as they will be visible by an observer in present time (10 Gyr after the SF beginning for constant SF, or (100 Myr, 1 Gyr, 5 Gyr, 10 Gyr after the SF beginning for burst SF). We omit issues related to obscuration or light propagation time.

² <http://universeathome.pl>

TABLE 3
FREQUENTLY USED ABBREVIATIONS

ULX	UltraLuminous X-ray source
BHULX	ULX with a BH accretor
NSULX	ULX with a NS accretor
PULX	Pulsing ULX
MS	Main Sequence
HG	H-rich Hertzsprung Gap
RG	Red Giant
CHeB	Core Helium Burning
HeS	Helium Star
evHeS	evolved Helium Star
SN	SuperNova
AIC	Accretion Induced Collapse
RL	Roche Lobe
RLOF	Roche Lobe OverFlow
MT	Mass Transfer
GR	Gravitational Radiation
SF	Star Formation
WD	White Dwarf
ONeWD	Oxygene-Neon WD

The "upper limit" accretion model

In addition to accretion model described in Sec. 2.1 we investigated a possibility that all mass may be transferred from the donor and efficiently accreted by the accretor, i.e.

$$\dot{M}_{\text{acc}} = \dot{M}_{\text{RLOF}}. \quad (\text{A2})$$

This corresponds to the highest accretion rate that could potentially occur in a given system, but is most likely not realistic for high \dot{M}_{RLOF} . Therefore, this model should be considered as a rough upper limit for accretion.

The X-ray luminosity is calculated as

$$L_X = \frac{\epsilon G M_{\text{BH/NS}} \dot{M}_{\text{RLOF}}}{R_{\text{acc}}} = \eta \dot{M}_{\text{RLOF}} c^2, \quad (\text{A3})$$

where ϵ is a conversion efficiency of gravitational energy into radiation equal 1.0 for a NS (surface accretion) and 0.5 for a BH (disk accretion), $M_{\text{BH/NS}}$ is the mass of the accretor, R_{acc} is the radius of a NS (assumed to be 10 km) or a BH (3 Schwarzschild radii, non-rotating BH), and η is the radiative efficiency of a standard thin disk equal ~ 0.2 for a NS and 1/12 for a BH (e.g., Shakura & Sunyaev 1973).

Models of the beaming

In addition to the beaming model described in Sec. 2.2 we investigated also the following models:

No beaming (BN)

For this model we assumed isotropic emission, therefore,

$$b = 1 \quad (\text{A4})$$

for all systems and all mass transfer rates.

Constant beaming, no saturation (B01)

We start with the simplest model of constant beaming, and we apply it to all sources. We consider only one case of $b = 0.1$ ($\theta \approx 52^\circ$) to compare it with more realistic prescriptions described below. Such a constant beaming will lower the total luminosity which is required for a source to be observed as a ULX to $b \times 10^{39} \text{ erg s}^{-1}$. This will generally increase the number of predicted ULX sources. On the other hand, $P_{\text{obs},b}$ will be lower for all systems, which will decrease this number. These two processes may make the predicted number of ULXs lower or higher in comparison to models without beaming.

Sądowski's model with saturation (BS)

This beaming prescription is based mainly on the results of theoretical and numerical analysis presented in Lasota et al. (2016) and based on the results of KORAL (Sądowski et al. 2014) GRRMHD simulations. They showed that super-Eddington disks never become geometrically thick, because the thickness of slim disk does not depend on the MT rate. Even for very high \dot{m} the ratio of photosphere height (H) to radius (R) is $H/R \lesssim 1.6$. We fitted a phenomenological model to approximate the relation between H/R and \dot{m} found by Lasota et al. (2016) (Fig. 4), and we obtained

TABLE 4
#ULX (BURST SFR)

Metallicity		Time since burst				const SFR
		100 Myr	1 Gyr	5 Gyr	10 Gyr	
Z_{\odot}	#ULX	4.0×10^2	1.8×10^1	9.5×10^{-1}	1.1×10^{-1}	9.3×10^0
	#BHULX	3.7×10^2	2.8×10^{-7}	–	–	3.8×10^0
	#NSULX	3.5×10^1	1.8×10^1	9.5×10^{-1}	1.1×10^{-1}	5.5×10^0
$Z_{\odot}/10$	#ULX	7.3×10^3	1.1×10^2	7.0×10^{-1}	7.5×10^{-2}	1.0×10^2
	#BHULX	7.2×10^3	4.0×10^0	–	–	9.2×10^1
	#NSULX	8.1×10^1	1.1×10^2	7.0×10^{-1}	7.5×10^{-2}	1.3×10^1
$Z_{\odot}/100$	#ULX	5.0×10^3	2.9×10^1	1.0×10^{-1}	5.0×10^{-7}	5.6×10^1
	#BHULX	4.9×10^3	–	–	–	5.1×10^1
	#NSULX	1.6×10^1	2.9×10^1	1.0×10^{-1}	5.0×10^{-7}	5.0×10^0

NOTE. — Number of ULXs (#ULX) in the reference model with a division on BHULXs (#BHULX) and NSULXs (#NSULX) for different population ages. Burst duration is 100 Myr.

$$\frac{H}{R} = \frac{1.6}{1 + \frac{4}{\dot{m}}} \quad (\text{A5})$$

for non-rotating BH accretion with non-saturated magnetic field. This relation corresponds to $R = 30 R_G$, but H/R should not be significantly larger for other radii. The equation shows a moderate photosphere height also for sub-Eddington MT rates. We used the same prescription for NS accretors.

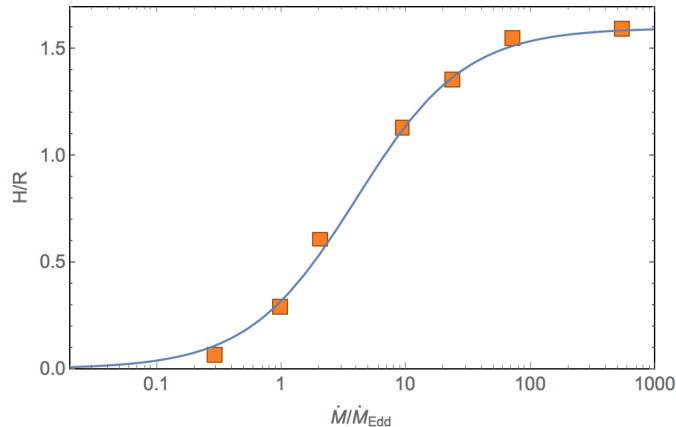


FIG. 4.— The ratio of photosphere height to disk radius (H/R) in relation to the mass transfer rate (in Eddington units). Orange squares represent the results of GRRMHD simulations with the use of KORAL code (Sądowski et al., private communication). The blue line shows the fit to the data (Eq. A5).

The H/R is related with the opening angle θ as

$$\left(\frac{H}{R}\right)^{-1} = \tan \frac{\theta}{2}, \quad (\text{A6})$$

which allows to derive the beaming factor as

$$b = 1 - \cos \frac{\theta}{2} \quad (\text{A7})$$

and the apparent isotropic luminosity is calculated as in Eq. 2.

The beaming becomes nearly constant for $\dot{m} \gtrsim 100$ what give the minimum opening angle $\theta_{\min} \approx 64^\circ$ ($b \approx 0.15$). The prescription works for the entire range of \dot{m} and shows a small collimation also for nearly-Eddington MT ($\dot{m} < 1$). However, below $\dot{m} \approx 0.12$ beaming factor is always greater than $b > 0.95$ ($\theta > 170^\circ$).

TABLE 5
#ULX($L_{X,\min}$) 100 Myr AFTER SF START

Metallicity		$L_{X,\min}$			
		$10^{39} \text{ erg s}^{-1}$	$3 \times 10^{39} \text{ erg s}^{-1}$	$10^{40} \text{ erg s}^{-1}$	$10^{41} \text{ erg s}^{-1}$
Z_{\odot}	#ULX	4.0×10^2	6.5×10^1	1.4×10^1	5.0×10^{-1}
	#BHULX	3.7×10^2	4.0×10^1	4.7×10^0	3.8×10^{-1}
	#NSULX	3.5×10^1	2.5×10^1	9.4×10^0	1.3×10^{-1}
$Z_{\odot}/10$	#ULX	7.3×10^3	1.9×10^3	2.0×10^2	1.2×10^1
	#BHULX	7.2×10^3	1.9×10^3	1.8×10^2	1.1×10^1
	#NSULX	8.1×10^1	4.0×10^1	1.2×10^1	4.3×10^{-1}
$Z_{\odot}/100$	#ULX	5.0×10^3	2.4×10^3	3.9×10^2	1.5×10^1
	#BHULX	4.9×10^3	2.4×10^3	3.8×10^2	1.5×10^1
	#NSULX	1.6×10^1	1.2×10^1	9.0×10^0	7.5×10^{-2}

NOTE. — Number of ULXs depending on the minimal luminosity ($L_{X,\min}$) for different metallicities with a division on BHULXs and NSULXs.

TABLE 6
NUMBER OF ULXs AND MAXIMAL LUMINOSITY FOR ALL SIMULATIONS

Model ^a	#ULX	Number per MWEGB ^b		$L_{X,\max}[\text{erg s}^{-1}]^c$	
		#BHULX	#NSULX	BHULX	NSULX
			Z_{\odot}		
AD0 BN	3.1×10^1	3.1×10^0 (10%)	2.8×10^1 (89%)	8.4×10^{44}	3.3×10^{44}
AD0 B01	1.8×10^2	1.1×10^0 (0%)	1.8×10^2 (99%)	8.4×10^{45}	3.3×10^{45}
AD0 BK	2.2×10^1	2.7×10^0 (12%)	1.9×10^1 (87%)	2.6×10^{47}	1.0×10^{47}
AD0 BS	2.0×10^1	2.3×10^0 (11%)	1.8×10^1 (88%)	5.5×10^{45}	2.2×10^{45}
AD1 BN	1.5×10^1	4.4×10^0 (29%)	1.1×10^1 (70%)	3.0×10^{40}	5.1×10^{39}
AD1 B01	2.0×10^2	1.5×10^0 (0%)	2.0×10^2 (99%)	3.0×10^{41}	5.1×10^{40}
AD1 BK	9.3×10^0	3.8×10^0 (41%)	5.5×10^0 (58%)	9.2×10^{42}	1.6×10^{42}
AD1 BS	2.0×10^1	2.9×10^0 (14%)	1.7×10^1 (85%)	2.0×10^{41}	3.4×10^{40}
			$Z_{\odot}/10$		
AD0 BN	1.6×10^2	9.4×10^1 (58%)	6.7×10^1 (41%)	6.8×10^{45}	2.3×10^{44}
AD0 B01	3.7×10^2	4.3×10^1 (11%)	3.3×10^2 (88%)	6.8×10^{46}	2.3×10^{45}
AD0 BK	1.3×10^2	8.4×10^1 (63%)	5.0×10^1 (36%)	2.1×10^{48}	7.1×10^{46}
AD0 BS	1.1×10^2	6.4×10^1 (60%)	4.1×10^1 (39%)	4.5×10^{46}	1.5×10^{45}
AD1 BN	1.3×10^2	1.1×10^2 (83%)	2.1×10^1 (16%)	8.6×10^{40}	4.5×10^{39}
AD1 B01	4.2×10^2	5.0×10^1 (11%)	3.7×10^2 (88%)	8.6×10^{41}	4.5×10^{40}
AD1 BK	1.0×10^2	9.2×10^1 (87%)	1.3×10^1 (12%)	2.7×10^{43}	1.4×10^{42}
AD1 BS	1.1×10^2	6.8×10^1 (61%)	4.2×10^1 (38%)	5.7×10^{41}	3.0×10^{40}
			$Z_{\odot}/100$		
AD0 BN	8.5×10^1	6.1×10^1 (72%)	2.3×10^1 (27%)	8.9×10^{45}	2.5×10^{44}
AD0 B01	8.6×10^1	1.4×10^1 (16%)	7.2×10^1 (83%)	8.9×10^{46}	2.5×10^{45}
AD0 BK	7.2×10^1	5.6×10^1 (78%)	1.6×10^1 (21%)	2.7×10^{48}	7.7×10^{46}
AD0 BS	4.9×10^1	3.8×10^1 (78%)	1.1×10^1 (21%)	5.9×10^{46}	1.6×10^{45}
AD1 BN	6.6×10^1	5.9×10^1 (89%)	7.2×10^0 (10%)	1.3×10^{41}	5.5×10^{39}
AD1 B01	8.0×10^1	1.6×10^1 (19%)	6.4×10^1 (80%)	1.3×10^{42}	5.5×10^{40}
AD1 BK	5.6×10^1	5.1×10^1 (91%)	5.0×10^0 (8%)	4.0×10^{43}	1.7×10^{42}
AD1 BS	5.0×10^1	3.7×10^1 (73%)	1.3×10^1 (26%)	8.6×10^{41}	3.6×10^{40}

^a AD0/1 - “upper limit”/logarithmic accretion model (Secs. A.1 and 2.1; BN/B01/BK/BS - beaming models (Secs. A.2 and 2.2).

^b Mikly-Way Equivalent Galaxy

^c The maximal obtained luminosity for the particular accretor.

TABLE 7
GENERAL PARAMETERS OF THE SIMULATIONAL RESULTS (BURST SFR 100 Myr AGO)

Model ^a	#ULX	Number per MWE ^a		$L_{X,\max}[\text{erg s}^{-1}]^b$	
		#BHULX	#NSULX	BHULX	NSULX
			Z_{\odot}		
AD0 BN	3.4×10^2	2.8×10^2 (83%)	5.8×10^1 (16%)	8.4×10^{44}	3.3×10^{44}
AD0 B01	4.7×10^2	9.3×10^1 (19%)	3.8×10^2 (80%)	8.4×10^{45}	3.3×10^{45}
AD0 BK	2.8×10^2	2.6×10^2 (90%)	2.8×10^1 (9%)	2.6×10^{47}	1.0×10^{47}
AD0 BS	2.8×10^2	2.1×10^2 (75%)	6.8×10^1 (24%)	5.5×10^{45}	2.2×10^{45}
AD1 B01	5.7×10^2	1.3×10^2 (22%)	4.4×10^2 (77%)	3.0×10^{41}	5.1×10^{40}
AD1 BK	4.0×10^2	3.7×10^2 (91%)	3.5×10^1 (8%)	9.2×10^{42}	1.6×10^{42}
AD1 BS	3.8×10^2	2.8×10^2 (75%)	9.4×10^1 (24%)	2.0×10^{41}	3.4×10^{40}
			$Z_{\odot}/10$		
AD0 BN	7.5×10^3	7.2×10^3 (96%)	2.9×10^2 (3%)	6.8×10^{45}	1.2×10^{44}
AD0 B01	3.0×10^3	3.0×10^3 (98%)	4.9×10^1 (1%)	6.8×10^{46}	1.2×10^{45}
AD0 BK	6.6×10^3	6.4×10^3 (98%)	1.2×10^2 (1%)	2.1×10^{48}	3.7×10^{46}
AD0 BS	5.2×10^3	5.1×10^3 (98%)	6.7×10^1 (1%)	4.5×10^{46}	7.9×10^{44}
AD1 BN	8.6×10^3	8.5×10^3 (98%)	1.0×10^2 (1%)	8.6×10^{40}	4.5×10^{39}
AD1 B01	3.9×10^3	3.8×10^3 (96%)	1.4×10^2 (3%)	8.6×10^{41}	4.5×10^{40}
AD1 BK	7.3×10^3	7.2×10^3 (98%)	8.1×10^1 (1%)	2.7×10^{43}	1.4×10^{42}
AD1 BS	5.7×10^3	5.6×10^3 (97%)	1.5×10^2 (2%)	5.7×10^{41}	3.0×10^{40}
			$Z_{\odot}/100$		
AD0 BN	5.9×10^3	5.9×10^3 (99%)	2.8×10^1 (0%)	8.9×10^{45}	2.1×10^{43}
AD0 B01	1.3×10^3	1.3×10^3 (99%)	4.4×10^0 (0%)	8.9×10^{46}	2.1×10^{44}
AD0 BK	5.4×10^3	5.4×10^3 (99%)	1.1×10^1 (0%)	2.7×10^{48}	6.5×10^{45}
AD0 BS	3.7×10^3	3.7×10^3 (99%)	6.9×10^0 (0%)	5.9×10^{46}	1.4×10^{44}
AD1 BN	5.7×10^3	5.7×10^3 (99%)	1.4×10^1 (0%)	1.3×10^{41}	5.5×10^{39}
AD1 B01	1.5×10^3	1.5×10^3 (96%)	4.9×10^1 (3%)	1.3×10^{42}	5.5×10^{40}
AD1 BK	5.0×10^3	4.9×10^3 (99%)	1.6×10^1 (0%)	4.0×10^{43}	1.7×10^{42}
AD1 BS	3.7×10^3	3.6×10^3 (98%)	5.8×10^1 (1%)	8.6×10^{41}	3.6×10^{40}

NOTE. — The same as in Tab. 6, but for burst SF which started 100 Myr ago and lasted for 100 Myr.

TABLE 8
GENERAL PARAMETERS OF THE SIMULATIONAL RESULTS (BURST SFR 1 Gyr AGO)

Model ^a	#ULX	Number per MWE ^a		$L_{X,\max}[\text{erg s}^{-1}]^b$	
		#BHULX	#NSULX	BHULX	NSULX
			Z_{\odot}		
AD0 BN	8.3×10^1	8.5×10^{-3} (0%)	8.3×10^1 (99%)	2.0×10^{42}	2.2×10^{42}
AD0 B01	3.9×10^2	3.6×10^{-1} (0%)	3.9×10^2 (99%)	2.0×10^{43}	2.2×10^{43}
AD0 BK	6.0×10^1	3.5×10^{-4} (0%)	6.0×10^1 (99%)	6.2×10^{44}	6.8×10^{44}
AD0 BS	5.5×10^1	1.5×10^{-3} (0%)	5.5×10^1 (99%)	1.3×10^{43}	1.4×10^{43}
AD1 BN	3.8×10^1	8.7×10^{-5} (0%)	3.8×10^1 (99%)	3.7×10^{39}	3.9×10^{39}
AD1 B01	5.2×10^2	1.2×10^{-1} (0%)	5.2×10^2 (99%)	3.7×10^{40}	3.9×10^{40}
AD1 BK	1.8×10^1	2.8×10^{-7} (0%)	1.8×10^1 (99%)	1.1×10^{42}	1.2×10^{42}
AD1 BS	8.0×10^1	1.3×10^{-5} (0%)	8.0×10^1 (99%)	2.4×10^{40}	2.6×10^{40}
			$Z_{\odot}/10$		
AD0 BN	6.8×10^2	4.1×10^0 (0%)	6.8×10^2 (99%)	4.8×10^{42}	1.4×10^{43}
AD0 B01	8.5×10^2	1.2×10^1 (1%)	8.4×10^2 (98%)	4.8×10^{43}	1.4×10^{44}
AD0 BK	5.7×10^2	3.9×10^0 (0%)	5.7×10^2 (99%)	1.5×10^{45}	4.3×10^{45}
AD0 BS	2.8×10^2	4.2×10^0 (1%)	2.8×10^2 (98%)	3.2×10^{43}	9.2×10^{43}
AD1 BN	1.2×10^2	4.0×10^0 (3%)	1.2×10^2 (96%)	9.0×10^{39}	3.5×10^{39}
AD1 B01	9.9×10^2	5.0×10^0 (0%)	9.8×10^2 (99%)	9.0×10^{40}	3.5×10^{40}
AD1 BK	1.1×10^2	4.0×10^0 (3%)	1.1×10^2 (96%)	2.8×10^{42}	1.1×10^{42}
AD1 BS	2.9×10^2	3.8×10^0 (1%)	2.9×10^2 (98%)	5.9×10^{40}	2.3×10^{40}
			$Z_{\odot}/100$		
AD0 BN	2.2×10^2	5.6×10^{-2} (0%)	2.2×10^2 (99%)	3.4×10^{42}	7.3×10^{42}
AD0 B01	1.7×10^2	1.6×10^0 (0%)	1.7×10^2 (99%)	3.4×10^{43}	7.3×10^{43}
AD0 BK	1.6×10^2	1.3×10^{-2} (0%)	1.6×10^2 (99%)	1.0×10^{45}	2.2×10^{45}
AD0 BS	7.2×10^1	1.1×10^{-2} (0%)	7.2×10^1 (99%)	2.2×10^{43}	4.8×10^{43}
AD1 BN	3.1×10^1	0.0×10^0 (0%)	3.1×10^1 (100%)	0.0×10^0	2.8×10^{39}
AD1 B01	2.2×10^2	0.0×10^0 (0%)	2.2×10^2 (100%)	0.0×10^0	2.8×10^{40}
AD1 BK	2.9×10^1	0.0×10^0 (0%)	2.9×10^1 (100%)	0.0×10^0	8.6×10^{41}
AD1 BS	6.3×10^1	0.0×10^0 (0%)	6.3×10^1 (100%)	0.0×10^0	1.8×10^{40}

NOTE. — The same as in Tab. 6, but for burst SF which started 1 Gyr ago and lasted for 100 Myr.

TABLE 9
GENERAL PARAMETERS OF THE SIMULATIONAL RESULTS (BURST SFR 5 Gyr AGO)

Model ^a	#ULX	Number per MWEG ^a		#NSULX	$L_{X,\max}[\text{erg s}^{-1}]^b$		
		#BHULX			BHULX	NSULX	
				Z_{\odot}			
AD0 BN	7.3×10^0	0.0×10^0	(0%)	7.3×10^0	(100%)	0.0×10^0	7.2×10^{43}
AD0 B01	6.6×10^1	0.0×10^0	(0%)	6.6×10^1	(100%)	0.0×10^0	7.2×10^{44}
AD0 BK	4.9×10^0	0.0×10^0	(0%)	4.9×10^0	(100%)	0.0×10^0	2.2×10^{46}
AD0 BS	3.5×10^0	0.0×10^0	(0%)	3.5×10^0	(100%)	0.0×10^0	4.7×10^{44}
AD1 BN	7.2×10^{-1}	0.0×10^0	(0%)	7.2×10^{-1}	(100%)	0.0×10^0	2.9×10^{39}
AD1 B01	5.0×10^1	0.0×10^0	(0%)	5.0×10^1	(100%)	0.0×10^0	2.9×10^{40}
AD1 BK	9.5×10^{-1}	0.0×10^0	(0%)	9.5×10^{-1}	(100%)	0.0×10^0	8.9×10^{41}
AD1 BS	2.0×10^0	0.0×10^0	(0%)	2.0×10^0	(100%)	0.0×10^0	1.9×10^{40}
				$Z_{\odot}/10$			
AD0 BN	6.7×10^0	0.0×10^0	(0%)	6.7×10^0	(100%)	0.0×10^0	9.4×10^{42}
AD0 B01	6.5×10^1	7.2×10^{-1}	(1%)	6.4×10^1	(98%)	6.1×10^{39}	9.4×10^{43}
AD0 BK	4.9×10^0	0.0×10^0	(0%)	4.9×10^0	(100%)	0.0×10^0	2.9×10^{45}
AD0 BS	4.4×10^0	0.0×10^0	(0%)	4.4×10^0	(100%)	0.0×10^0	6.2×10^{43}
AD1 BN	1.4×10^0	0.0×10^0	(0%)	1.4×10^0	(100%)	0.0×10^0	3.0×10^{39}
AD1 B01	5.1×10^1	0.0×10^0	(0%)	5.1×10^1	(100%)	0.0×10^0	3.0×10^{40}
AD1 BK	7.0×10^{-1}	0.0×10^0	(0%)	7.0×10^{-1}	(99%)	0.0×10^0	9.2×10^{41}
AD1 BS	3.2×10^0	0.0×10^0	(0%)	3.2×10^0	(100%)	0.0×10^0	2.0×10^{40}
				$Z_{\odot}/100$			
AD0 BN	1.9×10^0	0.0×10^0	(0%)	1.9×10^0	(100%)	0.0×10^0	1.2×10^{43}
AD0 B01	1.9×10^1	2.0×10^{-2}	(0%)	1.9×10^1	(99%)	6.8×10^{39}	1.2×10^{44}
AD0 BK	1.4×10^0	0.0×10^0	(0%)	1.4×10^0	(100%)	0.0×10^0	3.7×10^{45}
AD0 BS	2.0×10^0	0.0×10^0	(0%)	2.0×10^0	(100%)	0.0×10^0	7.9×10^{43}
AD1 BN	3.0×10^{-4}	0.0×10^0	(0%)	3.0×10^{-4}	(100%)	0.0×10^0	3.0×10^{39}
AD1 B01	4.9×10^0	1.2×10^{-1}	(2%)	4.8×10^0	(97%)	6.5×10^{39}	3.0×10^{40}
AD1 BK	1.0×10^{-1}	0.0×10^0	(0%)	1.0×10^{-1}	(100%)	0.0×10^0	9.2×10^{41}
AD1 BS	7.9×10^{-1}	0.0×10^0	(0%)	7.9×10^{-1}	(100%)	0.0×10^0	2.0×10^{40}

NOTE. — The same as in Tab. 6, but for burst SF which started 5 Gyr ago and lasted for 100 Myr.

TABLE 10
GENERAL PARAMETERS OF THE SIMULATIONAL RESULTS (BURST SFR 10 Gyr ago)

Model ^a	#ULX	Number per MWEG ^a #BHULX	#NSULX	$L_{X,\max}[\text{erg s}^{-1}]^b$	
				BHULX	NSULX
			Z_{\odot}		
AD0 BN	1.2×10^0	0.0×10^0 (0%)	1.2×10^0 (100%)	0.0×10^0	8.7×10^{42}
AD0 B01	8.1×10^0	0.0×10^0 (0%)	8.1×10^0 (100%)	0.0×10^0	8.7×10^{43}
AD0 BK	8.3×10^{-1}	0.0×10^0 (0%)	8.3×10^{-1} (100%)	0.0×10^0	2.7×10^{45}
AD0 BS	7.4×10^{-1}	0.0×10^0 (0%)	7.4×10^{-1} (100%)	0.0×10^0	5.7×10^{43}
AD1 BN	2.9×10^{-2}	0.0×10^0 (0%)	2.9×10^{-2} (100%)	0.0×10^0	3.0×10^{39}
AD1 B01	2.6×10^0	0.0×10^0 (0%)	2.6×10^0 (100%)	0.0×10^0	3.0×10^{40}
AD1 BK	1.1×10^{-1}	0.0×10^0 (0%)	1.1×10^{-1} (100%)	0.0×10^0	9.2×10^{41}
AD1 BS	3.6×10^{-1}	0.0×10^0 (0%)	3.6×10^{-1} (100%)	0.0×10^0	2.0×10^{40}
			$Z_{\odot}/10$		
AD0 BN	1.5×10^0	0.0×10^0 (0%)	1.5×10^0 (100%)	0.0×10^0	5.4×10^{42}
AD0 B01	1.2×10^1	0.0×10^0 (0%)	1.2×10^1 (100%)	0.0×10^0	5.4×10^{43}
AD0 BK	1.1×10^0	0.0×10^0 (0%)	1.1×10^0 (100%)	0.0×10^0	1.7×10^{45}
AD0 BS	9.4×10^{-1}	0.0×10^0 (0%)	9.4×10^{-1} (100%)	0.0×10^0	3.6×10^{43}
AD1 BN	2.1×10^{-1}	0.0×10^0 (0%)	2.1×10^{-1} (100%)	0.0×10^0	2.8×10^{39}
AD1 B01	7.3×10^0	0.0×10^0 (0%)	7.3×10^0 (100%)	0.0×10^0	2.8×10^{40}
AD1 BK	7.5×10^{-2}	0.0×10^0 (0%)	7.5×10^{-2} (100%)	0.0×10^0	8.6×10^{41}
AD1 BS	2.9×10^{-1}	0.0×10^0 (0%)	2.9×10^{-1} (100%)	0.0×10^0	1.8×10^{40}
			$Z_{\odot}/100$		
AD0 BN	6.2×10^{-1}	0.0×10^0 (0%)	6.2×10^{-1} (100%)	0.0×10^0	5.1×10^{42}
AD0 B01	5.9×10^0	0.0×10^0 (0%)	5.9×10^0 (100%)	0.0×10^0	5.1×10^{43}
AD0 BK	4.4×10^{-1}	0.0×10^0 (0%)	4.4×10^{-1} (100%)	0.0×10^0	1.6×10^{45}
AD0 BS	3.8×10^{-1}	0.0×10^0 (0%)	3.8×10^{-1} (100%)	0.0×10^0	3.4×10^{43}
AD1 BN	1.5×10^{-4}	0.0×10^0 (0%)	1.5×10^{-4} (100%)	0.0×10^0	2.8×10^{39}
AD1 B01	2.9×10^0	0.0×10^0 (0%)	2.9×10^0 (100%)	0.0×10^0	2.8×10^{40}
AD1 BK	5.0×10^{-7}	0.0×10^0 (0%)	5.0×10^{-7} (100%)	0.0×10^0	8.6×10^{41}
AD1 BS	2.3×10^{-5}	0.0×10^0 (0%)	2.3×10^{-5} (100%)	0.0×10^0	1.8×10^{40}

NOTE. — The same as in Tab. 6, but for burst SF which started 10 Gyr ago and lasted for 100 Myr. A total absence of BHULXs may be observed.

TABLE 11
COMPANIONS (CONSTANT SFR)

Model	MS	HG	RG	CHeB	HeMS	HeWD	HybWD	MS	HG	RG	HeMS	HeHG	HeGB	HeWD	COWD	HybWD
								Z_{\odot}								
AD0 BN	0.82	0.18	0.01					0.03	0.05	0.05	0.01	0.08		0.32	0.09	0.37
AD0 B01	0.91	0.07	0.02					0.02	0.02	0.01	0.16			0.38	0.10	0.32
AD0 BK	0.91	0.09						0.01	0.04	0.04	0.01	0.08		0.34	0.10	0.39
AD0 BS	0.92	0.08						0.01	0.06	0.03	0.03	0.09		0.33	0.09	0.35
AD1 BN	0.85	0.15						0.04	0.10	0.02	0.02	0.09	0.01	0.22	0.08	0.42
AD1 B01	0.94	0.05						0.05	0.04	0.01	0.15	0.01		0.33	0.10	0.32
AD1 BK	0.94	0.06						0.13	0.10	0.08	0.04	0.04		0.17	0.07	0.37
AD1 BS	0.94	0.06						0.09	0.16	0.05	0.02	0.08		0.23	0.08	0.30
								$Z_{\odot}/10$								
AD0 BN	0.68	0.30		0.01				0.06	0.47	0.02		0.01		0.21	0.07	0.17
AD0 B01	0.87	0.10						0.02	0.03		0.03			0.47	0.15	0.29
AD0 BK	0.74	0.24	0.01	0.01				0.03	0.51	0.01				0.21	0.07	0.16
AD0 BS	0.79	0.20	0.01	0.01				0.03	0.49	0.01		0.01		0.22	0.07	0.17
AD1 BN	0.69	0.28		0.02				0.10	0.39	0.02		0.02		0.19	0.08	0.21
AD1 B01	0.91	0.08						0.06	0.04	0.01	0.03			0.42	0.15	0.30
AD1 BK	0.76	0.21	0.01	0.01				0.11	0.54	0.05				0.13	0.05	0.13
AD1 BS	0.81	0.17	0.01	0.01				0.08	0.52	0.03		0.01		0.16	0.06	0.15
								$Z_{\odot}/100$								
AD0 BN	0.77	0.09		0.13	0.01			0.02	0.48	0.04		0.06		0.25	0.01	0.13
AD0 B01	0.89	0.04		0.06				0.03	0.03	0.03	0.07			0.56	0.03	0.25
AD0 BK	0.83	0.05		0.12				0.01	0.48	0.04		0.04		0.27	0.01	0.14
AD0 BS	0.87	0.05		0.08				0.02	0.29	0.12		0.04		0.35	0.02	0.18
AD1 BN	0.76	0.10		0.13	0.01			0.04	0.45	0.05		0.13		0.14	0.01	0.18
AD1 B01	0.91	0.04		0.05				0.13	0.05	0.06	0.07			0.33	0.03	0.31
AD1 BK	0.84	0.06		0.10				0.12	0.47	0.20		0.03		0.07	0.01	0.10
AD1 BS	0.89	0.05		0.06				0.10	0.36	0.27		0.03		0.11	0.01	0.12

NOTE. — Companions (donors) in ULXs formed in models with constant SFR. Fractions for different companion types are provided separately for BHULXs and NSULXs.

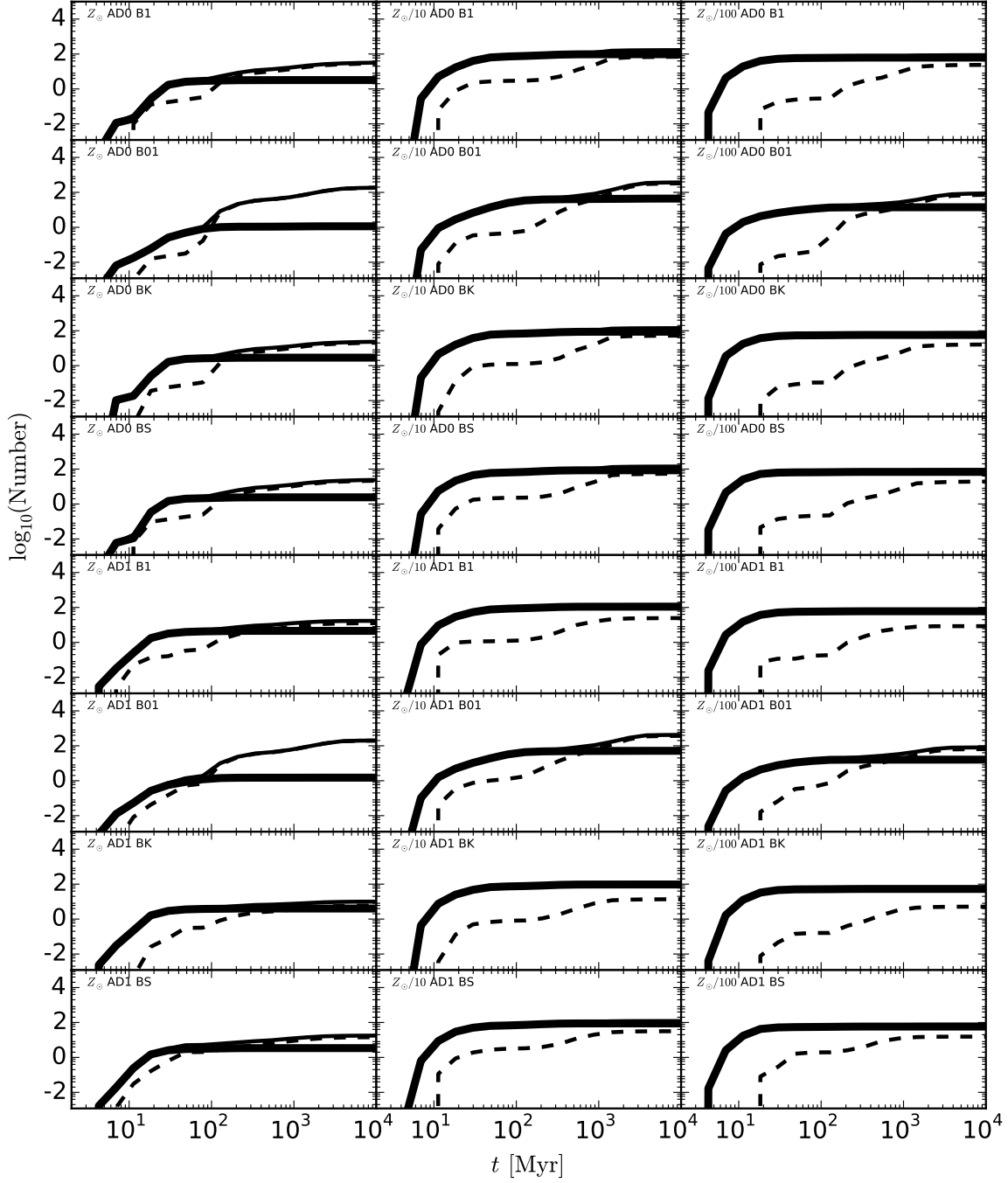


FIG. 5.— The relation between the number of ULXs and the age of the population for constant SFR of $4.4 M_{\odot} \text{ yr}^{-1}$ (total stellar mass equal Milky-Way Equivalent Galaxy). The thick line corresponds to BHULXs, dashed to NSULXs, and solid to all ULXs. Z_{\odot} depicts the solar metallicity, AD0/1 are the accretion models (Secs. A.1 and 2.1) and BN,B01,BK,BS stand for beaming models (Secs. A.2 and 2.2).

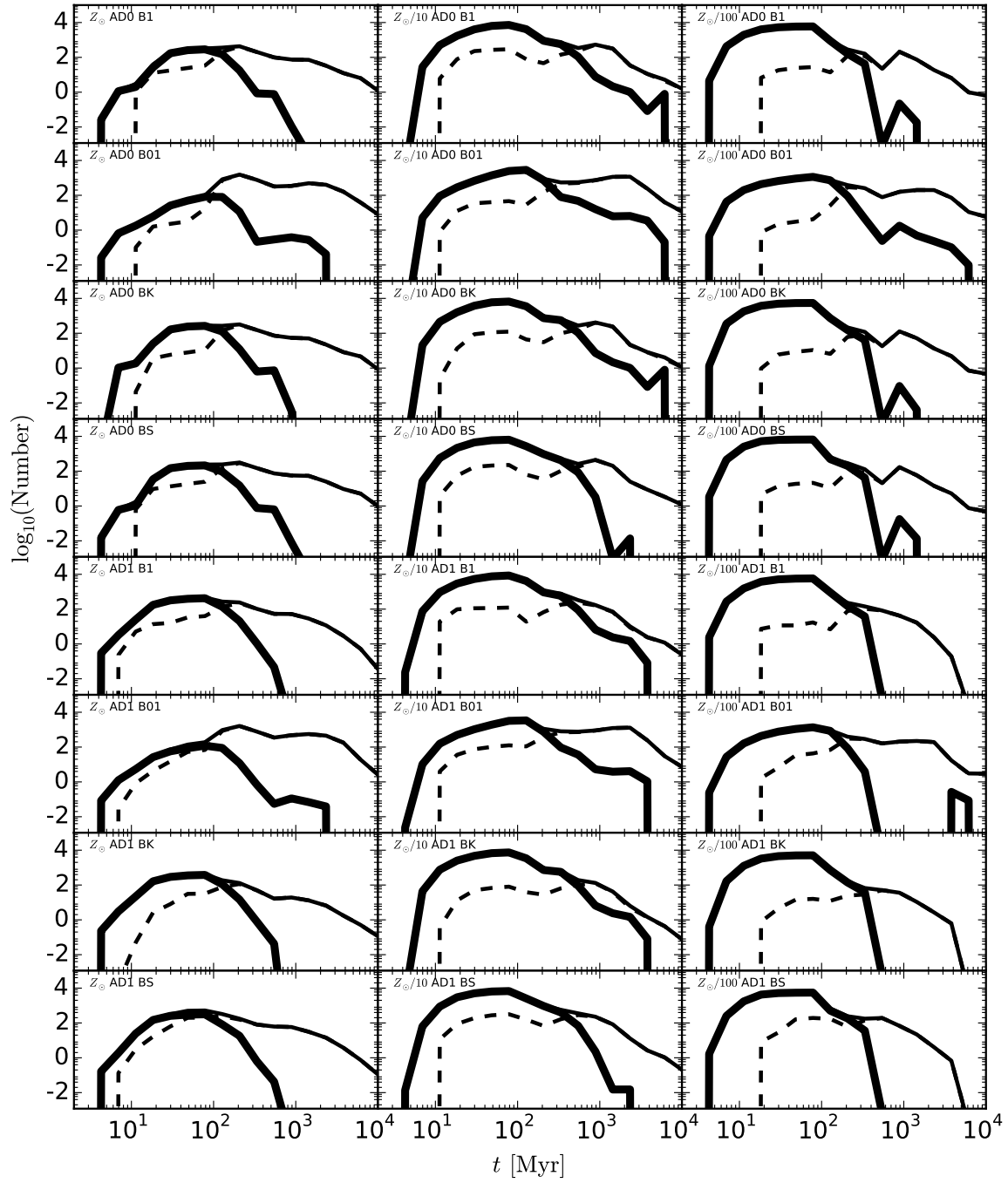


FIG. 6.— The same as in Fig. 5, but for burst star-formation with a duration of 100 Myr and SFR of $440 M_{\odot} \text{ yr}^{-1}$.

TABLE 12
COMPANIONS (100 SFR)

Model	MS	HG	RG	CHeB	HeMS	HeWD	HybWD	MS	HG	RG	HeMS	HeHG	HeGB	HeWD	COWD	HybWD
Z_{\odot}																
AD0 BN	0.89	0.11						0.42			0.02	0.49	0.01			0.06
AD0 B01	0.96	0.03						0.01			0.98	0.01				
AD0 BK	0.97	0.03						0.29			0.04	0.57				0.10
AD0 BS	0.97	0.03						0.07			0.67	0.22				0.03
AD1 BN	0.90	0.10						0.28				0.59	0.12			
AD1 B01	0.97	0.03						0.14			0.85	0.01				
AD1 BK	0.98	0.02						0.89				0.10				
AD1 BS	0.97	0.03						0.73			0.11	0.15	0.01			
$Z_{\odot}/10$																
AD0 BN	0.86	0.11		0.02	0.01			0.98			0.01	0.01				
AD0 B01	0.97	0.03						0.97			0.02	0.01				
AD0 BK	0.94	0.04		0.01				0.98			0.02	0.01				
AD0 BS	0.95	0.03		0.01				0.96			0.03	0.01				
AD1 BN	0.85	0.12		0.03	0.01			0.94			0.01	0.04	0.02			
AD1 B01	0.97	0.03		0.01				0.99			0.01					
AD1 BK	0.94	0.03		0.02				1.00								
AD1 BS	0.95	0.04		0.01				0.99								
$Z_{\odot}/100$																
AD0 BN	0.81	0.05		0.13	0.01			0.97				0.02				
AD0 B01	0.91	0.02		0.06				0.88			0.10	0.01				
AD0 BK	0.86	0.01		0.12				0.98			0.01	0.01				0.01
AD0 BS	0.90	0.02		0.08				0.85			0.12	0.01				0.01
AD1 BN	0.79	0.06		0.14	0.01			0.60				0.27	0.13			
AD1 B01	0.92	0.02		0.05				0.98			0.01	0.01				
AD1 BK	0.87	0.02		0.11				1.00								
AD1 BS	0.92	0.02		0.06				0.98				0.02				

NOTE. — Companions (donors) in ULXs formed in models with burst SF. Start of the burst was 100 Myr ago and its duration was 100 Myr.

TABLE 13
COMPANIONS (1000 SFR)

Model	MS	HG	RG	CHeB	HeMS	HeWD	HybWD	MS	HG	RG	HeMS	HeHG	HeGB	HeWD	COWD	HybWD
Z_{\odot}																
AD0 BN		1.00						0.02	0.07					0.49	0.09	0.33
AD0 B01	0.28	0.43	0.29					0.07	0.03					0.12	0.03	0.74
AD0 BK		1.00						0.01	0.07					0.49	0.09	0.33
AD0 BS		1.00						0.02	0.12					0.46	0.08	0.31
AD1 BN			1.00					0.01	0.31		0.01			0.35	0.07	0.25
AD1 B01	0.51	0.01	0.47		0.01			0.15	0.17	0.02				0.09	0.02	0.54
AD1 BK			1.00					0.03	0.41		0.01			0.29	0.06	0.20
AD1 BS			1.00					0.04	0.47					0.26	0.05	0.17
$Z_{\odot}/10$																
AD0 BN	0.40	0.37	0.18					0.01	0.74					0.17	0.03	0.05
AD0 B01	0.32	0.44	0.23					0.03	0.08					0.32	0.05	0.51
AD0 BK	0.41	0.34	0.19						0.78					0.15	0.03	0.05
AD0 BS	0.40	0.37	0.18					0.01	0.58					0.28	0.05	0.08
AD1 BN	0.60	0.10	0.24					0.04	0.47					0.33	0.06	0.11
AD1 B01	0.64	0.22	0.13					0.08	0.11					0.28	0.05	0.47
AD1 BK	0.60	0.10	0.24					0.03	0.73	0.01				0.15	0.03	0.05
AD1 BS	0.58	0.12	0.25					0.02	0.63	0.01				0.23	0.04	0.07
$Z_{\odot}/100$																
AD0 BN		0.87	0.03	0.10					0.79					0.17	0.01	0.03
AD0 B01	0.12	0.47	0.38				0.03	0.01	0.10	0.01				0.36	0.01	0.51
AD0 BK		1.00							0.79					0.17	0.01	0.03
AD0 BS		0.90	0.02	0.07					0.60					0.32	0.02	0.05
AD1 BN									0.46	0.02				0.43	0.03	0.07
AD1 B01								0.19	0.08	0.02				0.29	0.01	0.42
AD1 BK								0.12	0.57	0.10				0.17	0.01	0.03
AD1 BS								0.05	0.46	0.12				0.30	0.02	0.04

NOTE. — Companions (donors) in ULXs formed in models with burst SF. Start of the burst was 1 Gyr ago and its duration was 100 Myr.

TABLE 14
COMPANIONS (5000 SFR)

Model	MS	HG	RG	CHeB	HeMS	HeWD	HybWD	MS	HG	RG	HeMS	HeHG	HeGB	HeWD	COWD	HybWD
									Z_{\odot}							
AD0 BN										0.37				0.63		
AD0 B01										0.01				0.75	0.24	
AD0 BK										0.32				0.68		
AD0 BS										0.19				0.81		
AD1 BN										0.31				0.69		
AD1 B01										0.02				0.63	0.35	
AD1 BK										0.78				0.22		
AD1 BS										0.61				0.39		
									$Z_{\odot}/10$							
AD0 BN										0.16				0.56	0.28	
AD0 B01								0.01		0.02				0.70	0.27	
AD0 BK										0.17				0.55	0.28	
AD0 BS										0.21				0.53	0.26	
AD1 BN										0.02				0.43	0.54	
AD1 B01								0.01		0.04				0.54	0.41	
AD1 BK										0.25				0.34	0.41	
AD1 BS										0.38				0.28	0.34	
									$Z_{\odot}/100$							
AD0 BN								0.10		0.25				0.66		
AD0 B01						1.00		0.02	0.03	0.17				0.77		
AD0 BK								0.04		0.30				0.66		
AD0 BS								0.02		0.60				0.38		
AD1 BN										1.00						
AD1 B01						0.17		0.09	0.10	0.68				0.08		
AD1 BK								0.38		0.62						
AD1 BS								0.03		0.97						

NOTE. — Companions (donors) in ULXs formed in models with burst SF. Start of the burst was 5 Gyr ago and its duration was 100 Myr.

TABLE 15
COMPANIONS (10000 SFR)

Model	MS	HG	RG	CHeB	HeMS	HeWD	HybWD	MS	HG	RG	HeMS	HeHG	HeGB	HeWD	COWD	HybWD
									Z_{\odot}							
AD0 BN										0.40				0.60		
AD0 B01										0.08				0.92		
AD0 BK										0.38				0.62		
AD0 BS										0.40				0.60		
AD1 BN										0.19				0.81		
AD1 B01										0.31				0.69		
AD1 BK										0.92				0.08		
AD1 BS										0.91				0.09		
									$Z_{\odot}/10$							
AD0 BN														0.83	0.17	
AD0 B01										0.07				0.73	0.20	
AD0 BK														0.83	0.17	
AD0 BS														0.83	0.17	
AD1 BN														0.89	0.11	
AD1 B01										0.11				0.56	0.34	
AD1 BK														0.90	0.10	
AD1 BS														0.89	0.11	
									$Z_{\odot}/100$							
AD0 BN														1.00		
AD0 B01								0.05	0.07	0.12				0.54		
AD0 BK														1.00		
AD0 BS														1.00		
AD1 BN										1.00						
AD1 B01								0.11	0.13	0.27				0.01		
AD1 BK										1.00						
AD1 BS										1.00						

NOTE. — Companions (donors) in ULXs formed in models with burst SF. Start of the burst was 10 Gyr ago and its duration was 100 Myr. A total absence of BHULXs may be observed.